



Cite this: *Phys. Chem. Chem. Phys.*,  
2016, **18**, 10528

# Towards understanding the improved stability of palladium supported on TS-1 for catalytic combustion†

Adi Setiawan,<sup>ab</sup> Jarrod Friggieri,<sup>a</sup> Hadi Hosseiniamoli,<sup>a</sup> Eric M. Kennedy,<sup>a</sup>  
Bogdan Z. Dlugogorski,<sup>c</sup> Adesoji A. Adesina<sup>d</sup> and Michael Stockenhuber<sup>\*a</sup>

A novel Pd supported on TS-1 combustion catalyst was synthesized and tested in methane combustion under very lean and under highly humid conditions (<1%). A notable increase in hydrothermal stability was observed over 1900 h time-on-stream experiments, where an almost constant, steady state activity obtaining 90% methane conversion was achieved below 500 °C. Surface oxygen mobility and coverage plays a major role in the activity and stability of the lean methane combustion in the presence of large excess of water vapour. We identified water adsorption and in turn the hydrophobicity of the catalyst support as the major factor influencing the long term stability of combustion catalysts. While Pd/Al<sub>2</sub>O<sub>3</sub> catalyst shows a higher turn-over frequency than that of Pd/TS-1 catalyst, the situation reversed after ca. 1900 h on stream. Two linear regions, with different activation energies in the Arrhenius plot for the equilibrium Pd/TS-1 catalyst, were observed. The conclusions were supported by catalyst characterization using H<sub>2</sub>-chemisorption, TPD, XPS analyses as well as N<sub>2</sub>-adsorption-desorption, XRD, SEM, TEM. The hydrophobicity and competitive adsorption of water with oxygen is suggested to influence oxygen surface coverage and in turn the apparent activation energy for the oxidation reaction.

Received 15th January 2016,  
Accepted 10th March 2016

DOI: 10.1039/c6cp00319b

www.rsc.org/pccp

## 1. Introduction

Catalytic combustion of methane is a potential solution to mitigate methane emissions as it can operate outside the flammability range and production of NO<sub>x</sub> is essentially absent due to its relatively low reaction temperatures. Supported Pd catalysts are considered to be excellent catalysts for this reaction.<sup>1</sup> Poisoning by water and other contaminants can have long-term deleterious effects, and significantly reduce the potential for their use in catalytic combustion of fugitive methane emission from coal mines ventilation air.<sup>2</sup>

Earlier studies reported that water significantly inhibits the activity of Pd on Al<sub>2</sub>O<sub>3</sub><sup>3,4</sup> and Pd on zeolites<sup>5,6</sup> at lower temperatures, which is due to competition between water and methane for adsorption on catalyst active sites.<sup>3,4,7</sup> Furthermore,

an irreversible deactivation can be induced by the presence of water where the active site (palladium oxide) transforms into a less active site (palladium hydroxide).<sup>3,4,7</sup> Ciuparu *et al.*, suggested that the hydroxyl groups produced by the methane combustion reaction are bound strongly on the surface<sup>8</sup> and accumulate on the support.<sup>9</sup> Therefore, when external water is introduced the surface becomes saturated and the rate of desorption is decreased.<sup>8</sup>

In addition to its well defined, crystalline microporous nature and redox activity, the TS-1 zeotype is known as a more hydrophobic material compared to other zeolites.<sup>10</sup> Due to their microporous and well defined pore structure, zeolites often are used to support redox functionalities because of their ability to stabilise small clusters. The titanium silicalite-1 (TS-1) materials initially prepared by Taramasso *et al.* were effectively used as a catalyst for the selective oxidation of alkenes and alcohol substrates using hydrogen peroxide.<sup>11–13</sup> Using photoassisted deposition (PAD) method, nanosize Pd particles were successfully deposited on TS-1 and tested for direct synthesis of H<sub>2</sub>O<sub>2</sub> from H<sub>2</sub> and O<sub>2</sub>.<sup>14</sup> Very recently, the preparation of Au–Pd nano-particles supported on hierarchical TS-1 catalysts was evaluated for selective oxidation of benzyl alcohol using *in situ* generated hydrogen peroxide.<sup>15</sup> It was found that the use of TS-1 as catalyst support improved metal dispersion.<sup>15</sup> It is generally agreed that the dispersion of the noble metal is one of the key factors for

<sup>a</sup> Priority Research Centre for Energy (PRCfE), Discipline of Chemical Engineering, School of Engineering, The University of Newcastle, Callaghan, NSW 2308, Australia. E-mail: Michael.Stockenhuber@newcastle.edu.au;

Fax: +61 2 4921 6893; Tel: +61 2 4985 4433

<sup>b</sup> Mechanical Engineering Department, Faculty of Engineering,

Universitas Malikussaleh, Bukit Indah, Lhokseumawe, 24352, Indonesia

<sup>c</sup> School of Engineering and Information Technology, Murdoch University, Murdoch, WA 6150, Australia

<sup>d</sup> ATODATECH LLC, Brentwood, CA 94513, USA

† Electronic supplementary information (ESI) available. See DOI: 10.1039/c6cp00319b

improving the activity of palladium catalysts for methane oxidation.<sup>1</sup> These properties are thought to improve the long term stability of a combustion catalyst and thus we investigated TS-1 as a support material for palladium catalysts under long-term reaction conditions. To our knowledge, for catalytic combustion of lean methane mixtures, palladium supported on TS-1 has not been previously reported.

Attempts to improve the tolerance against water poisoning were undertaken by supporting palladium on composite materials such as LaMnO<sub>3</sub>-ZrO<sub>2</sub><sup>16</sup> and TiO<sub>2</sub>-SiO<sub>2</sub>.<sup>17</sup> As reported in the literature,<sup>17</sup> mixing titanium and silica oxides avoids or delays the reaction between Pd and H<sub>2</sub>O. A hydrothermal stability test was reported recently by Liu *et al.*<sup>4</sup> using Ni-modified alumina as support at a reaction temperature of 600 °C. Our recent work on a long term stability test (1150 h) over Pd/Al<sub>2</sub>O<sub>3</sub> catalyst disclosed that the level of 90% methane conversion is achievable at temperatures ≤ 500 °C in the presence of water in the feed.<sup>2</sup>

For the current work, we prepared a new palladium catalyst using titanium silicalite (TS-1) zeolite as support for methane combustion to gain a better understanding of the underlying principles that govern catalyst stability. The resistance of this catalyst was evaluated during catalytic combustion of lean methane in air over an extended period of time. The long term stability test was performed under conditions where the level of methane conversion was maintained at or above 90% at a gas hourly space velocity of 100 000 h<sup>-1</sup>. The physical and chemical properties of Pd/TS-1 catalyst were investigated in order to understand the advantages of this catalyst in comparison with conventional palladium on alumina catalysts.

## 2. Experimental

### 2.1 Catalyst preparation

Catalyst containing 1.4 wt% Pd/TS-1 was prepared by wet impregnation of a commercial titanium silicalite (TS-1) support (ENI-Polimeri Europa SpA) with an aliquot of Pd(II) nitrate solution (10 wt% in 10 wt% nitric acid, Sigma-Aldrich) mixed using a mortar and pestle. Water was added drop-wise while mixing, until a paste was formed. The resulting paste was dried in an oven at 110 °C for approximately 20 h. The dried catalyst was then ground, pressed and sieved to 250–425 μm. A tubular fixed-bed reactor was employed for the calcination of the dried solid catalyst in air at 500 °C for 2 h followed by purging in helium while slowly cooling the catalyst to desired reaction temperature. For comparison, a commercially available 1.0 wt% Pd/Al<sub>2</sub>O<sub>3</sub> (Sigma-Aldrich) was used and activated in air at 500 °C for 4 h followed by purging in H<sub>2</sub> for 2 h.<sup>2</sup> In contrast to our previous investigation Pd/TS-1 catalyst was activated in air only. Thus, it is expected Pd<sup>2+</sup> is the only species observed over the used sample.

### 2.2 Catalyst characterization

The surface areas of the catalysts were measured by nitrogen adsorption at 77 K using a Gemini 11 2370 surface area analyzer. A volumetric glass apparatus was employed to assess

the active particle size and metal dispersion by performing hydrogen chemisorption at 35 °C, in the pressure range between 30 and 90 mbar (vacuum measurement by Pfeiffer CMR 362-TPG 261, data logging by LabVIEW version 7.1.1). A H/Pd = 1/1 stoichiometry was assumed for H<sub>2</sub> chemisorption on metallic palladium.<sup>18</sup> Mean particle diameter was estimated based on dispersion values using the following formula:<sup>19</sup>

$$dp = \frac{6 \times C_a \times M \times 10^9}{\rho \times D \times N_a}$$

where  $C_a$  is concentration of surface metal atom (equal to  $1.27 \times 10^{19}$  atoms m<sup>-2</sup>),<sup>19</sup>  $M$  is Pd atomic mass,  $\rho$  is Pd volumetric mass (equal to  $12.02 \times 10^6$  g m<sup>-3</sup>),<sup>19</sup>  $D$  is metal dispersion and  $N_a$  is Avogadro number. Temperature-programmed desorption (TPD) analysis was undertaken using a purpose built TPD apparatus with a Pfeiffer Prisma quadrupole mass analyser for detection. Zeiss Sigma VP FESEM served to capture the scanning electron microscopy (SEM) images of the sample using a secondary electron (SE) detector and backscattered electron (BE) detector. A JEOL 2200 FS transmission electronic microscope (TEM) with EDS and a scanning transmission electron microscope (STEM) system was used for imaging nano-sized Pd particles and support as well as measuring the particle size distribution. Palladium loading was quantified using a Varian 715-ES inductively coupled plasma optical emission spectrometer (ICP-OES). Powder X-ray diffraction patterns of catalysts were examined using Cu K $\alpha$  radiation with a Philips X'Pert diffractometer. Diffractograms were collected in the  $2\theta$  angle range from 2° to 90° with 0.008°  $2\theta$  step resolution.

For surface analysis, X-ray photoelectron spectroscopy (XPS) was conducted using monochromated Al K alpha (energy 1486.68 eV) radiation and the emitted photoelectrons were analyzed using an ESCALAB250Xi manufactured by Thermo Scientific, UK. To minimize the possibility of sample contamination, spent samples were immediately transferred into sealed containers after stopping the reaction by cooling in helium. The sample was mounted on the stub using indium tape. The energy scale of the XPS spectra was referenced to the adventitious carbon adsorption at 284.6 eV. The spectrometer was calibrated against binding energies of Au 4f<sub>7/2</sub> = 83.96 eV, Ag 3d<sub>5/2</sub> = 368.21 eV and Cu 2p<sub>3/2</sub> = 932.62 eV.

### 2.3 Catalytic activity assessment

The activity of the catalyst was measured in a tubular, stainless steel micro reactor. The inlet mixture was 7000 ppm CH<sub>4</sub>, 3.2 vol% H<sub>2</sub>O balanced with air at a gas hourly space velocity (GHSV) of 100 000 h<sup>-1</sup>. The inlet and outlet gas mixtures were analyzed using an online gas chromatograph equipped with a thermal conductivity detector (TCD) and concentric-packed single column (Alltech CTR-1). The reactant mixture was passed through a saturator and a humidity probe was installed at the outlet. The reaction temperature was measured with a K-type thermocouple placed into the catalyst bed.

For catalytic stability studies, a second, separate reactor set-up was used and operated continuously under varying reaction conditions (temperature was increased in order to achieve a 90%

level of conversion for methane). Throughout the study, the feed concentration of methane and carbon dioxide were kept constant at 7000 ppm and 10 000 ppm, respectively. The saturator system was operated at ambient temperature ( $25\text{ }^{\circ}\text{C} \pm 3\text{ }^{\circ}\text{C}$ ) resulting in a relative humidity of *ca.* 85% (corresponding to a  $\text{H}_2\text{O}_{(\text{v})}$  pressure of between 30 000–40 000 ppm). This humidity is well within the range of a typical coal mine as reported in the literature.<sup>20</sup> The targeted 90% methane conversion was maintained by increasing the catalyst bed temperature as the catalyst deactivated during time on stream up to 1900 h.

Kinetic measurements were carried out over the fresh and long-term used catalysts using a wet feed containing 7000 ppm  $\text{CH}_4$ , 3.2%  $\text{H}_2\text{O}$  balanced with air. Carbon dioxide was not added to the feed since the reaction rate is independent of the partial pressure of  $\text{CO}_2$ .<sup>21</sup> The turn-over frequency (TOF), defined as the moles of methane converted per second and per mole of active site was calculated under conditions where the methane conversion level was below 15%. The number of active sites on the catalyst was estimated based on palladium dispersion measurements. Pd dispersion was also calculated based on the average Pd particle size measured by TEM analysis (for fresh and used catalysts) using the formula mentioned above.

### 3. Results and discussion

#### 3.1 Catalyst activity and stability under wet feed conditions

In addition to catalytic activity measurements in the micro-reactor, the surface reactions involved in methane combustion over the Pd/TS-1 were studied using temperature programmed desorption (TPD). The sample was heated under vacuum at  $500\text{ }^{\circ}\text{C}$  for 1 h to remove any pre-adsorbed compounds. At  $110\text{ }^{\circ}\text{C}$ , methane (99.99%) was adsorbed. Subsequently, the products were desorbed and the gas phase was analysed. During the desorption experiments, a significant quantity of  $\text{CO}_2$  was produced, suggesting methane is being oxidised by lattice oxygen of the catalyst. This result suggests that the surface oxygen participates in the methane oxidation reaction, following a Mars–van Krevelen mechanism under these conditions.<sup>22,23</sup> Fig. 1 shows TPD profiles of  $\text{CO}_2$  ( $m/z = 44$ ) desorbed from Pd/TS-1 catalyst. TPD spectra indicate that a significant rate of desorption of  $\text{CO}_2$  was detected at temperatures ranging from  $270\text{ }^{\circ}\text{C}$  to  $400\text{ }^{\circ}\text{C}$  with a maximum desorption rate at  $395\text{ }^{\circ}\text{C}$ . It is expected that in the plug-flow reactor study, methane oxidation can utilize lattice oxygen from the catalyst over this temperature range.

The catalytic performance of Pd/TS-1 catalyst was measured for total oxidation of methane in the presence of water vapour in the feed. For initial activation, the catalyst was calcined in air at  $500\text{ }^{\circ}\text{C}$  for 2 h then cooled to  $200\text{ }^{\circ}\text{C}$  in a flow of helium. A feed of 7000 ppm methane and 3.2 vol%  $\text{H}_2\text{O}$  in air was passed through the catalyst bed with a GHSV of  $100\,000\text{ h}^{-1}$ . The experiment was started by gradually increasing the furnace temperature. The performance of the catalyst was evaluated in terms of turn-over frequencies in the range of 2–11% methane conversion level, and it has been normalized by the number of

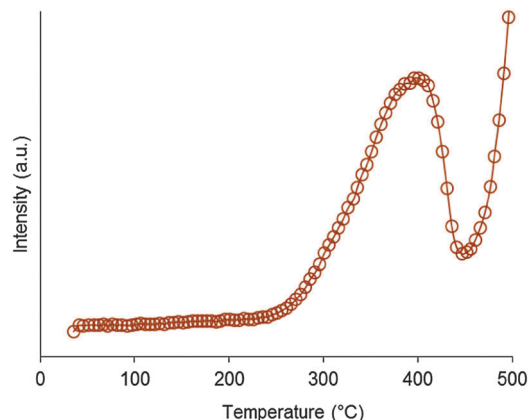


Fig. 1 TPD spectra of  $\text{CO}_2$  ( $m/z = 44$ ) desorbed from Pd/TS-1 catalysts.  $\text{CO}_2$  was produced under vacuum on the surface of catalysts subsequent to  $\text{CH}_4$  *in situ* adsorption at  $110\text{ }^{\circ}\text{C}$  in presence of water. Heating ramp =  $5\text{ }^{\circ}\text{C min}^{-1}$ .

active sites measured by TEM analysis. Fig. 2 shows the Arrhenius plots for Pd/TS-1 catalyst. As a comparison, the activity of Pd/ $\text{Al}_2\text{O}_3$  catalyst was tested under similar conditions and also plotted in Fig. 2. Table 1 summarises the kinetic data of both catalysts. Comparison of the Arrhenius plots shows that over palladium supported on TS-1 catalysts a lower rate per active site compared to Pd/ $\text{Al}_2\text{O}_3$  catalyst was observed. Note that a TS-1 sample (without Pd loading) was also tested under similar condition as described previously and conversion of methane was not detected at temperatures as high as  $510\text{ }^{\circ}\text{C}$  confirming that TS-1 zeolite itself is not an active catalyst for methane oxidation under our reaction conditions. The deposited palladium particles on TS-1 are responsible for converting methane to carbon dioxide.

In the presence of water in the feed, the turn-over frequencies of fresh Pd/TS-1 and Pd/ $\text{Al}_2\text{O}_3$  catalysts at reaction temperature of  $312\text{ }^{\circ}\text{C}$  were  $0.007\text{ s}^{-1}$  and  $0.015\text{ s}^{-1}$ , respectively. Estimation of the apparent activation energy resulted in  $247\text{ kJ mol}^{-1}$  for Pd/TS-1 compared to  $159\text{ kJ mol}^{-1}$  for Pd/ $\text{Al}_2\text{O}_3$  catalyst.

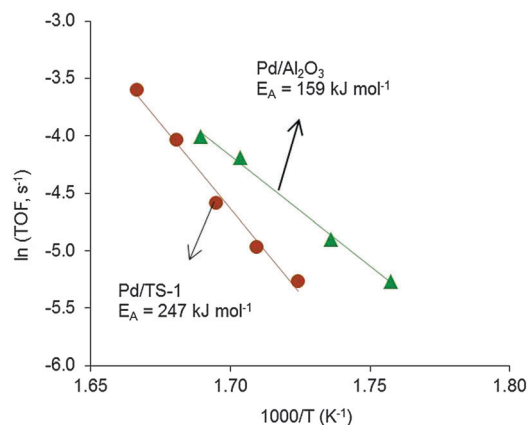


Fig. 2 The Arrhenius plots of Pd/TS-1 and Pd/ $\text{Al}_2\text{O}_3$  catalysts under wet feed conditions. The reactions were run under feed conditions consisting of 7000 ppm  $\text{CH}_4$ , 3.2 vol%  $\text{H}_2\text{O}$  in air at GHSV =  $100\,000\text{ h}^{-1}$ . ● = Pd/TS-1; ▲ = Pd/ $\text{Al}_2\text{O}_3$ .

**Table 1** Kinetic data for Pd/TS-1 and Pd/Al<sub>2</sub>O<sub>3</sub> catalysts

Samples	$E_a$ (kJ mol <sup>-1</sup> )	TOF (s <sup>-1</sup> )
Pd/TS-1, fresh	247	0.007 <sup>a</sup>
Pd/Al <sub>2</sub> O <sub>3</sub> , fresh	159	0.015 <sup>a</sup>
Pd/TS-1, used	269 ( $E_1$ ) and 48 ( $E_2$ )	0.066 <sup>b</sup>
Pd/Al <sub>2</sub> O <sub>3</sub> , used	128	0.120 <sup>b</sup>

<sup>a</sup> TOF was calculated at temperature of 312 °C. <sup>b</sup> TOF was calculated at temperature of 365 °C.

The activation energy of the conversion over the fresh Pd/Al<sub>2</sub>O<sub>3</sub> catalyst is consistent with the data reported in the literature<sup>21,23</sup> where under humid conditions (feed containing 2–2.5% H<sub>2</sub>O) the apparent activation energies were in the range of 150–166 kJ mol<sup>-1</sup>. The apparent activation energies reported are similar for alumina and zirconia supported catalysts and in turn little influence of metal support interactions are expected for our alumina supported catalyst as well.

The reaction rate measurement reported in the literature was also not affected by external diffusion and the close comparison with our activation energies suggests the absence of diffusion as well. Indeed, our own experimental diffusion test did not show a significant influence of flow rates on conversion. Changing the flow rate and keeping space velocity constant resulted in a variation of the conversion from 6.4% to 6.9% (within the experimental error) when the flow rate was changed from 80 ml min<sup>-1</sup> to 120 ml min<sup>-1</sup> under a steady state conversion at a GHSV of 100 000 h<sup>-1</sup>. Internal diffusion for the TS-1 catalyst is possible, but the Thiele modulus was significantly smaller than 1 (0.11) clearly suggesting (together with the lack of external diffusion) the absence of Knudsen diffusion.<sup>24</sup> Pore diffusion was checked by altering the pellet size of 250–425 μm and 425–500 μm which resulted in a rate of 4.6 × 10<sup>-3</sup> mol s<sup>-1</sup> g<sub>cat</sub><sup>-1</sup> (308 °C) and 4.9 × 10<sup>-3</sup> mol s<sup>-1</sup> g<sub>cat</sub><sup>-1</sup> (310 °C), respectively. This indicates no observable effect of pore diffusion on the activity of the catalyst.

The activation barrier over the Pd/TS-1 and Pd/Al<sub>2</sub>O<sub>3</sub> catalysts is significantly high under conditions when the combustion gas was saturated with water vapour. A possible explanation for this behaviour can be related to the availability of labile oxygen for the combustion. As indicated above, the catalytic combustion can utilise stored surface oxygen and thus a Mars–van Krevelen type mechanism will be relevant in the temperature window studied. Clear evidence can be found in Fig. 1, where the reaction with methane and the absence of any oxidant results in the formation of CO<sub>2</sub>, suggesting the reaction of methane occurs with stored surface oxygen. Evidence for the existence of mobile, stored oxygen can also be observed in oxygen desorption shown in Fig. 5. The “effective” surface coverage of oxygen is expected to be higher than at lower temperatures. Competitive adsorption between O<sub>2</sub> and H<sub>2</sub>O is expected to have an effect, which would result in lower oxygen surface coverage over the Pd/Al<sub>2</sub>O<sub>3</sub> catalyst, in turn resulting in a smaller rate constant. However, increasing the reaction temperature will result in a reduced relative coverage of water/O<sub>2</sub> (heat of adsorption of water on supported Pd catalysts is lower than that of oxygen<sup>25,26</sup>) only

partially offsetting the effect of the increased availability of oxygen. A change in activation energy was attributed to the stability of PdO under varying conditions which goes hand in hand with a change in the reaction order of water in the kinetic expression.<sup>23</sup> This behaviour is consistent with our observations of the importance of oxygen coverage on the activity.

To assess the usefulness of the catalytic system for a practical application, evaluation of catalyst stability of the Pd/TS-1 was performed using a separate reactor configuration which was operated continuously under varying reaction temperatures in order to maintain a 90% level of methane conversion. The feed composition for these long term stability tests was adjusted, mimicking the ventilation air composition typically emitted from a coal mine (7000 ppm CH<sub>4</sub>; 10 000 ppm CO<sub>2</sub>; 30 000 to 40 000 ppm H<sub>2</sub>O balance air). Fig. 3 shows the catalyst bed reactor temperature of Pd/TS-1 over 1900 h.

It has been confirmed previously that the water vapour present in the feed would be the primary factor for catalyst deactivation in addition to the water vapour produced from reaction.<sup>2</sup> As plotted in Fig. 3, the initial temperature to achieve 90% conversion ( $T_{90}$ ) was 430 °C and the bed temperature was then slowly increased to maintain the methane conversion level. The bed temperature appears to plateau starting from 160 h until 1900 h time-on-stream. Hydroxyl group accumulation on the active site, carbon deposits and the increase in reaction temperature resulted in a slowly alteration of the oxygen surface coverage. This argument is supported by our TPD data as discussed below. To evaluate the performance of the catalyst under conditions relevant to the combustion of ventilation air methane under practically relevant conditions, data over Pd/TS-1 catalyst is compared with data that was reported earlier over Pd supported on alumina catalysts<sup>2</sup> and plotted in Fig. 3. It can be observed that the practical benchmark of 90% conversion can be maintained at lower temperatures over TS-1 supported compared to alumina supported Pd catalysts.

The Arrhenius plots of Pd/TS-1 and Pd/Al<sub>2</sub>O<sub>3</sub> measured following long-term time on stream experiments are plotted in Fig. 4. Our estimation of the rate of reaction over used Pd/TS-1 and Pd/Al<sub>2</sub>O<sub>3</sub> catalysts at 365 °C results in the TOF of 0.066 s<sup>-1</sup>

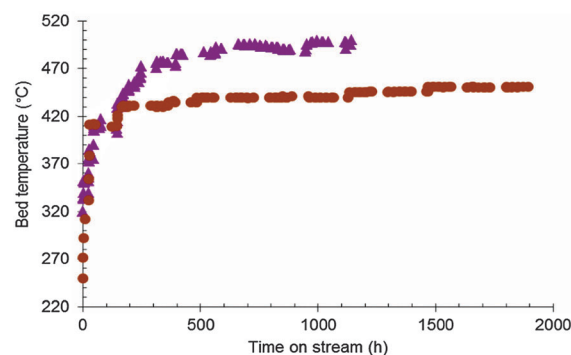


**Fig. 3** Catalyst bed temperature required for 90% CH<sub>4</sub> conversion over Pd/TS-1 and Pd/Al<sub>2</sub>O<sub>3</sub> catalysts. Feed: 7000 ppm CH<sub>4</sub>, 10 000 ppm CO<sub>2</sub>, 30 000–40 000 ppm H<sub>2</sub>O balance air, GHSV 100 000 h<sup>-1</sup>. ▲ = TOS experiment over Pd/Al<sub>2</sub>O<sub>3</sub>; ● = TOS experiment over Pd/TS-1.

and  $0.120 \text{ s}^{-1}$ , respectively. It is observed that over the used Pd/TS-1 catalyst the slope of the line (and in turn the apparent activation energy) changes at *ca.*  $360 \text{ }^\circ\text{C}$ , while over the used Pd/Al<sub>2</sub>O<sub>3</sub> catalyst no change in the apparent activation energy was observed. At reaction temperatures below  $360 \text{ }^\circ\text{C}$ , the Arrhenius plot of Pd/TS-1 suggests the activation energy is  $369 \text{ kJ mol}^{-1}$ . Above this reaction temperature, the activation energy decreases to  $48 \text{ kJ mol}^{-1}$ . In principle, this behaviour can be due to (i) diffusion effects, (ii) change in the mechanism and (iii) due to coverage dependency of the apparent activation enthalpy.<sup>27</sup> As mentioned above, external diffusion can be excluded since no variation of the conversion was observed upon changing the flow rate. It is also suggested that internal diffusion for the TS-1 catalyst is negligible. Furthermore, the reduction in apparent activation energy is significantly larger than 50%, also suggesting the absence of internal diffusion.<sup>28</sup>

The changes in activation energy in methane combustion over supported noble metal catalysts have been reported in the literature.<sup>24,28,29</sup> It was found that at lower temperatures, higher activation energies were observed which was suggested to be related to the heat of adsorption of oxygen on precious metal. The apparent higher activation energy at lower temperatures may be expressed as the sum of activation energies for oxidation of palladium and for methane oxidation by the resulting palladium oxide.<sup>28</sup> As shown in Fig. 5, oxygen TPD from Pd on TS-1 (after co-adsorption with water at  $300 \text{ }^\circ\text{C}$ ) discloses a desorption peak of O<sub>2</sub> at *ca.*  $480 \text{ }^\circ\text{C}$  whereas this peak was not observed over Pd on alumina subject to the same conditions. This suggests that at a reaction temperature of  $365 \text{ }^\circ\text{C}$ , most of the labile oxygen will have desorbed reducing the surface coverage of oxygen. This in turn (as suggested in ref. 27) results in a decreasing apparent activation energy, as was observed in Fig. 4. The Arrhenius plot of the used Pd/TS-1 catalyst also suggests that the water molecules on the surface of Pd/TS-1 catalyst start to desorb at temperature of  $360 \text{ }^\circ\text{C}$  resulting in an increase in rate of reaction. No accumulation of hydroxyl is expected at this temperature which is supported by

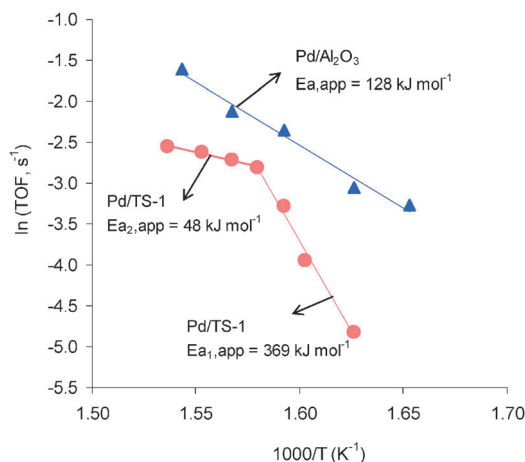


Fig. 4 The Arrhenius plots of Pd/TS-1 and Pd/Al<sub>2</sub>O<sub>3</sub> catalysts measure after long-term stability tests (used catalysts). The reactions were run under wet feed conditions consisting of 7000 ppm CH<sub>4</sub>, 3.2 vol% H<sub>2</sub>O in air at GHSV =  $100\,000 \text{ h}^{-1}$ . ● = used Pd/TS-1 and ▲ = used Pd/Al<sub>2</sub>O<sub>3</sub>.

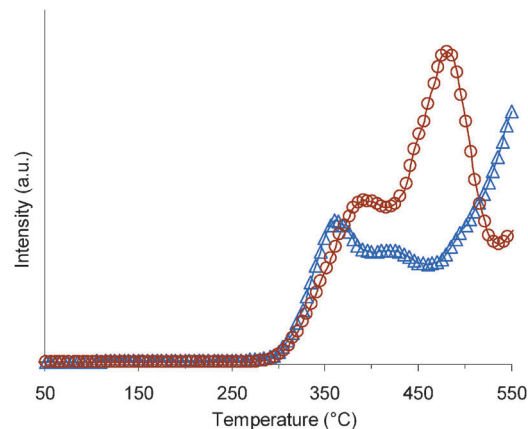


Fig. 5 TPD spectra of oxygen ( $m/z = 32$ ) desorbed from Pd/Al<sub>2</sub>O<sub>3</sub> and Pd/TS-1 catalysts. Oxygen was co-adsorbed with H<sub>2</sub>O at  $300 \text{ }^\circ\text{C}$ . Heating ramp =  $5 \text{ }^\circ\text{C min}^{-1}$ . ▲ = Pd/Al<sub>2</sub>O<sub>3</sub>; ● = Pd/TS-1.

TPD spectra as plotted in Fig. 6 and 7. On the other hand, TPD spectra of water desorbed from Pd/Al<sub>2</sub>O<sub>3</sub> catalyst at temperatures  $< 500 \text{ }^\circ\text{C}$  shows a very high intensity of water adsorbed on the surface of catalyst which persistently inhibits the reaction.

### 3.2 Characterization of catalysts

The surface properties of Pd/TS-1 in comparison with Pd/Al<sub>2</sub>O<sub>3</sub> catalysts were investigated utilizing TPD of oxygen. Prior to analysis, the sample was pre-treated under vacuum at  $500 \text{ }^\circ\text{C}$  for 1 h at a heating ramp of  $5 \text{ }^\circ\text{C min}^{-1}$ . Oxygen was co-adsorbed with H<sub>2</sub>O at  $300 \text{ }^\circ\text{C}$  and desorbed at  $550 \text{ }^\circ\text{C}$ . Fig. 5 shows the oxygen TPD spectra ( $m/z = 32$ ) of Pd/TS-1. In the presence of water, Fig. 5 shows that maximum rate of O<sub>2</sub> desorption over Pd/TS-1 was observed at  $480 \text{ }^\circ\text{C}$  whereas in contrast over Pd/Al<sub>2</sub>O<sub>3</sub> no peak was observed at this temperature range. These observations can be interpreted that the oxygen adsorption capacity is higher on the Pd/TS-1 catalyst. Similar phenomena were reported in the literature where high dispersion of the palladium on the support resulted in a higher oxygen mobility.<sup>30</sup> As observed from TEM and chemisorption results, the Pd dispersion is larger on Pd/TS-1 compared to Pd/Al<sub>2</sub>O<sub>3</sub> catalyst. The support has also been suggested to influence on the ability of palladium to adsorb oxygen and there was a strong

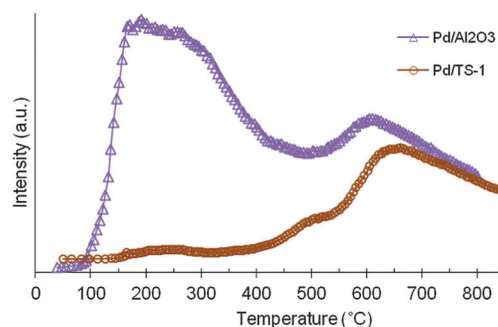


Fig. 6 TPD curves of water desorption from Pd/TS-1 and Pd/Al<sub>2</sub>O<sub>3</sub> catalysts. H<sub>2</sub>O was adsorbed at  $110 \text{ }^\circ\text{C}$ . Heating ramp =  $5 \text{ }^\circ\text{C min}^{-1}$ . ● = Pd/TS-1; ▲ = Pd/Al<sub>2</sub>O<sub>3</sub>.

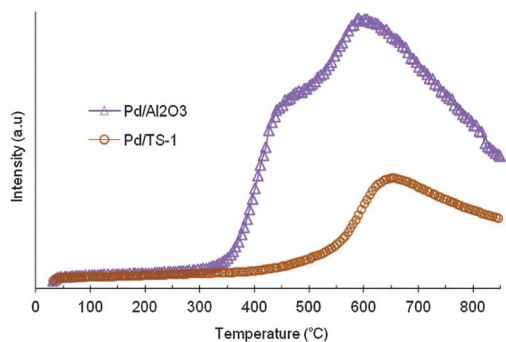


Fig. 7 TPD curves of water desorption from Pd/TS-1 and Pd/Al<sub>2</sub>O<sub>3</sub> catalysts after heating at 350 °C for 1 h. H<sub>2</sub>O adsorption at 110 °C. Heating ramp = 5 °C min<sup>-1</sup>. ○ = Pd/TS-1; △ = Pd/Al<sub>2</sub>O<sub>3</sub>.

correlation between the oxygen adsorption capacity of precious metal and its catalytic activity.<sup>28,31</sup>

The effect of water vapour on palladium supported on TS-1 catalyst was investigated using TPD analysis. Water was selected as the adsorbate with the purpose of investigating the interactions between water, active sites and the support material. The intensity of water ( $m/z = 18$ ) desorbed from the support material (pure TS-1) and Pd/TS-1 catalyst are provided in Fig. S1 of ESI.† Prior to adsorption, both samples were pre-heated for 1 h at 500 °C with a heating rate of 5 °C min<sup>-1</sup> to remove any pre-adsorbed compounds. Water was adsorbed at 110 °C to avoid any weakly bound adsorbate retained on the sample. Fig. S5 of ESI† suggests that the TPD spectra of Pd/TS-1 are identical to what was observed in water desorption from the unmodified TS-1 support material. There are high and low temperature desorption peaks observed in both samples spectra. A low intensity peak detected at 240 °C indicates that there is a small number of water molecules adsorbed on the catalyst surface. The higher temperature peaks appearing at 510 °C and 660 °C are attributed to desorption of surface hydroxyl groups resulting in partial destruction of the lattice suggested in the literature.<sup>32–34</sup>

Fig. 6 shows the comparison of TPD spectra of water desorbed from Pd/Al<sub>2</sub>O<sub>3</sub> and Pd/TS-1 catalysts. The TPD spectra of Pd/Al<sub>2</sub>O<sub>3</sub> suggest the presence of multiple desorption peaks at temperature below 500 °C and a higher desorption state at 610 °C. The area of the low temperature water desorption peak from Pd/Al<sub>2</sub>O<sub>3</sub> is much bigger compared to the higher temperature peak (ratio = 0.73/0.27). Our data suggests that Pd/Al<sub>2</sub>O<sub>3</sub> catalyst adsorbs more water at lower temperature, while Pd/TS-1 catalyst shows significantly reduced adsorption capacity for water at lower temperatures, which are relevant for the catalytic methane combustion.

Further investigation of the H<sub>2</sub>O-TPD phenomena were carried-out over Pd/TS-1 and Pd/Al<sub>2</sub>O<sub>3</sub> catalysts by adsorbing

water at 110 °C and heating to 350 °C for 1 h, then cooling to room temperature. TPD analysis started from room temperature increasing to a temperature of 850 °C. Prior to these experiments, both catalysts were heated under vacuum at 500 °C for 1 h. The spectra of H<sub>2</sub>O desorbed from both catalysts are plotted in Fig. 7. This plot discloses a significant desorption peak at 450 °C over Pd/Al<sub>2</sub>O<sub>3</sub> catalyst highlighting a stronger adsorption state of water on the surface. The opposite behaviour is observed from Pd/TS-1 catalyst, where no significant peak was detected at temperature below 500 °C.

The complexity of water adsorption–desorption for MFI-zeolitic adsorbents has been reported in the literature, especially for TS-1, ZSM-5 and silicalite-1 (pure silica).<sup>10</sup> It was found that among these zeolites, TS-1 is the most demonstrably hydrophobic material. It was reported that for hydrocarbons adsorption, TS-1 exhibited behaviour similar to that of ZSM-5 zeolite, however for water adsorption the intensity of TS-1 was as low as the rate of water desorbed from pure silica.<sup>10</sup> This argument is in line with what has been observed in TPD curves plotted in Fig. 6 and 7. TS-1 has very low concentration of adsorbed water and in turn helps to maintain the stability of Pd active sites during reaction. The hydrophobicity of TS-1 was suggested due to the absence of surface acidity (strong acid and hydrogen bonding), instead of an increased dispersion interaction.<sup>35</sup> More recent investigation also reported that the hydrophobic properties of TS-1 is due to the titanium atoms in the tetrahedral position of the MFI structure which create the hydrophobic environment.<sup>10</sup>

The adsorption and desorption of nitrogen was performed on pure TS-1 support, Pd/TS-1 and Pd/Al<sub>2</sub>O<sub>3</sub> catalysts in order to measure the surface area and the pore sizes. The adsorption–desorption isotherm of Pd/TS-1 and Pd/Al<sub>2</sub>O<sub>3</sub> catalysts are plotted in Fig. S2 of the ESI.† The textural properties of all samples tested are provided in Table 2.

In general, the isotherm adsorption plots of our samples fall into type-IV as classified by IUPAC which is typically the behaviour of mesoporous materials.<sup>36</sup> Interestingly, the desorption curves of Pd/TS-1 catalyst (Fig. S2a of ESI†) is shifted slightly to a higher volume over the pressure range while Pd/Al<sub>2</sub>O<sub>3</sub> catalyst desorption plot (Fig. S2b of ESI†) is shifted only at a relative pressure higher than 0.7. As reported in the literature, these shifts indicate enhanced adsorption over the range of relative pressures, which suggests the coexistence of micro and mesopores within these catalysts.<sup>37</sup> As shown in Table 2, the average mesopore diameter calculated using Barrett–Joyner–Halenda (BJH) method results in 5.4 nm and 16.8 nm for Pd/TS-1 and Pd/Al<sub>2</sub>O<sub>3</sub> catalysts, respectively. Not surprisingly the surface area of Pd/TS-1 catalyst is much higher compared to Pd supported on alumina catalyst,

Table 2 N<sub>2</sub>-physorption calculation results

Parameter	Sample				
	TS-1	Pd/TS-1	Used Pd/TS-1	Pd/Al <sub>2</sub> O <sub>3</sub>	Used Pd/Al <sub>2</sub> O <sub>3</sub>
Langmuir surface area (m <sup>2</sup> g <sup>-1</sup> )	641.9	492.8	476	212.9	146.5
BJH average pore diameter (Å)	30.7	54.1	23.6	167.6	158.7
BJH adsorption pore volume (cm <sup>3</sup> g <sup>-1</sup> )	0.07	0.11	0.06	0.66	0.4

due to the microporous nature of TS-1. The surface area estimated by Langmuir method discloses a decrease from  $641.9 \text{ m}^2 \text{ g}^{-1}$  to  $492.8 \text{ m}^2 \text{ g}^{-1}$  in the presence the Pd nano-particles on TS-1 which suggests the deposition of some Pd in the pores of the TS-1 support.

Nitrogen physisorption analysis over the used Pd/TS-1 catalyst suggests that the surface area decreased only *ca.* 3% after 1900 h time-on-stream experiment. In contrast, a significant loss in surface area was observed over the used Pd/Al<sub>2</sub>O<sub>3</sub> catalyst where the surface area decreased from  $212.9 \text{ m}^2 \text{ g}^{-1}$  to  $146.5 \text{ m}^2 \text{ g}^{-1}$  (*ca.* 31% drop) after 1100 h TOS experiment.

The crystallinity of palladium supported on TS-1 was investigated using powder X-ray diffraction (XRD) analysis. Fig. S3 of ESI† shows XRD patterns for Pd/TS-1 catalyst in comparison to XRD pattern of pure TS-1 support material. Diffraction reflections of both samples confirm the presence of MFI-type zeolite structure and high crystallinity of these samples.<sup>10,15</sup> A very small, broad reflection at  $34.8^\circ 2\theta$  observed in the XRD pattern of calcined Pd/TS-1 catalyst suggesting the existence of palladium oxide (0 1 2) reflection on the TS-1 support. This is consistent with a low net metal loading (from ICP-OES result) and indicates the well-dispersed nature of palladium particles on TS-1 zeolite (from H<sub>2</sub>-chemisorption result). The low intensity (high FWHM) of PdO reflections does not enable an estimation of the palladium particle size. An estimation of the active particle size calculated from the results of H<sub>2</sub>-chemisorption at 35 °C shows that average particle diameter is 7.6 nm resulting in 14.8% dispersion. A comparable result was obtained from hydrogen chemisorption of Pd/Al<sub>2</sub>O<sub>3</sub> catalyst which is suggesting a palladium dispersion of 14.2% with an average particle size of 7.9 nm.

Exploring the possibility of a morphological transformation during catalyst preparation and methane oxidation was carried out using scanning electron microscopy (SEM). Fig. 8 shows SEM images of TS-1 zeolite and Pd/TS-1 catalysts at the same magnifications. The topography of fresh TS-1 zeolite was captured by a secondary electron (SE) detector and shown in Fig. S4 of ESI.† Using a backscattered electron (BE) detector, the images of TS-1 support material and Pd/TS-1 catalyst were captured as shown in Fig. 8a and b. Comparing both images, SEM micrograph of fresh Pd/TS-1 catalyst reveals very small, brighter particles distributed over the whole area of TS-1 surface which are interpreted as signal from palladium particles. In this image, the palladium particle is recognized as the brighter particle due to its higher atomic weight (see the arrows). This has been confirmed by energy dispersive spectroscopy (EDS) which was performed during analysis. A less bright particle distribution is observed from Pd/Al<sub>2</sub>O<sub>3</sub> SEM image (see Fig. 8c). These images suggest that the nature of TS-1 support helps in establishing a better palladium particle distribution. This is in agreement to what has been reported in the literature that the morphology and microstructure of nano-sized Pd particle is affected by the nature of its support.<sup>4</sup>

The SEM images of fresh and used Pd/TS-1 catalysts are compared in Fig. S5 of ESI.† It can be seen that no significant measurable change in morphology was observed under SEM. This is consistent with N<sub>2</sub>-physisorption results where only 3% of surface area decreased during 1900 h TOS experiment.

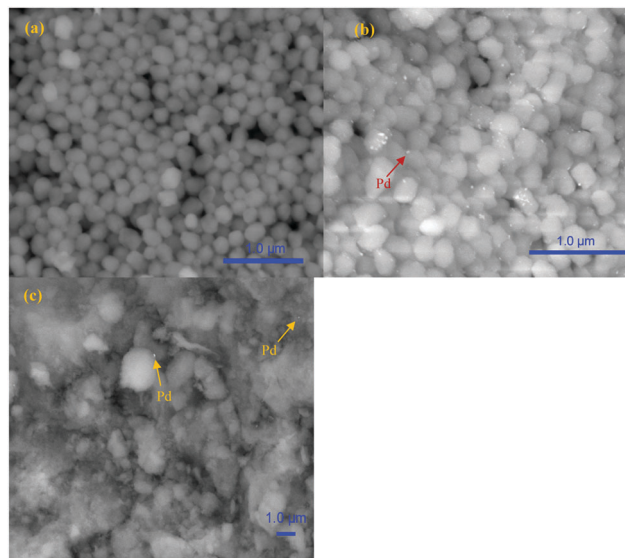


Fig. 8 SEM images of (a) TS-1 zeolite; (b) Pd/TS-1; and (c) Pd/Al<sub>2</sub>O<sub>3</sub> catalyst.

This minor change is most-likely related to the transformation of palladium particle. This argument is further substantiated by our finding from TEM analysis. It is suggested that the formation and removal of hydroxide compounds from the surface of catalyst can potentially accelerate the sintering process,<sup>38</sup> either sintering of the catalyst or support material.<sup>39</sup> The surface diffusion of the single phase solid is significantly increased at temperatures near to the Hüttig temperature ( $0.2\text{--}0.3 \times$  melting point).<sup>38</sup> Assuming the melting point of palladium is 1552 °C, the Hüttig temperature is then in the range of 310 °C to 466 °C. In Fig. 3 we can see that after 150 h, the bed temperatures were increased from 410 °C to 430 °C which is inside the Hüttig temperature range, and thus, a surface diffusion of palladium nano-particle would be expected.

Palladium particle size and distribution of Pd/TS-1 catalyst was observed under transmission electron microscope (TEM) before and after long-term stability test. Fig. 9a shows the representative TEM micrograph of fresh catalyst, including particle size distribution plot and the representative image of the used catalyst is provided in Fig. 9b. According to our statistical analysis, the size of palladium particle distributed on the surface of the fresh catalyst ranged from 1 nm to 11 nm with the average size of 4 nm. An increase in particle size was observed over the used catalyst, where the average particle size of palladium was 8 nm. This increase is most likely related to the deactivation observed over 1900 h time-on-stream experiment. A similar phenomena was reported over Pd/Al<sub>2</sub>O<sub>3</sub> catalyst, where the particle size of palladium increased after long-term stability test under wet feed conditions.<sup>2</sup> In Fig. 9c and d, the representative TEM images and particle distribution of fresh and used Pd/Al<sub>2</sub>O<sub>3</sub> catalysts are shown. The average Pd particle size of Pd/Al<sub>2</sub>O<sub>3</sub> catalyst increased from 2.6 nm to 8.2 nm after high humidity, long time-on-stream catalyst evaluation.

XPS spectra of fresh and used Pd/TS-1 catalyst are displayed in Fig. 10. The binding energies (BE) and surface composition

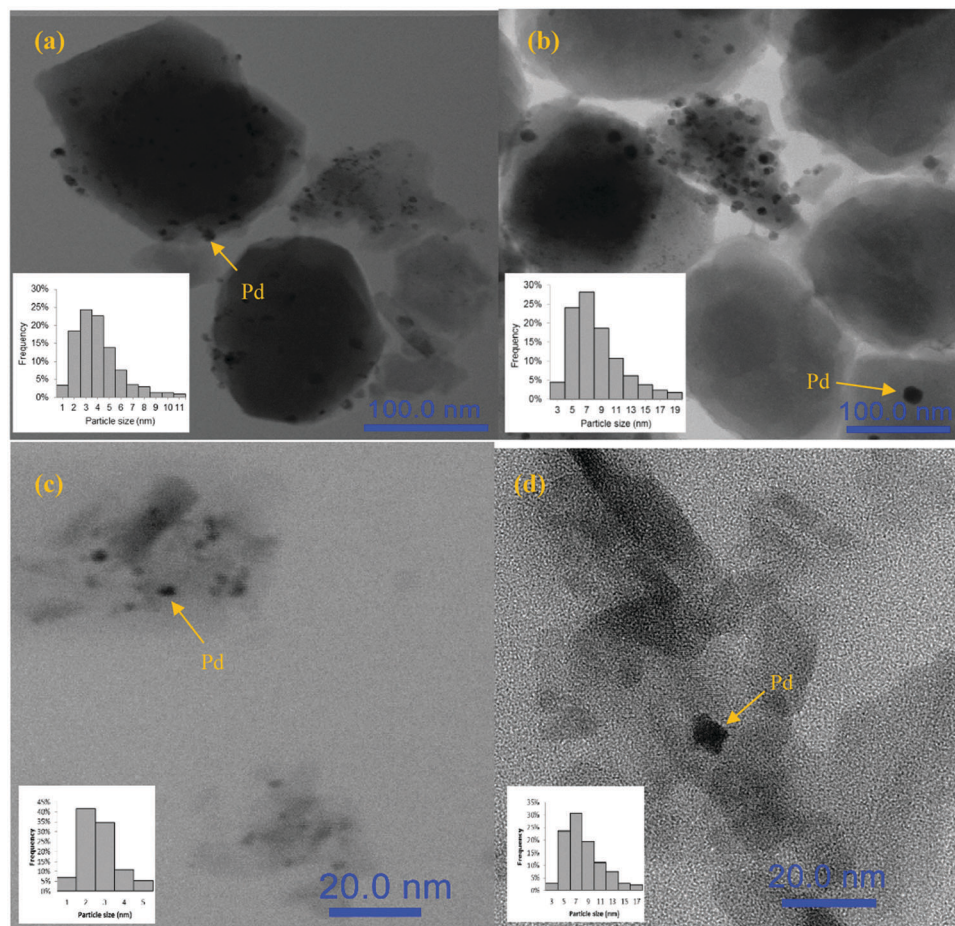


Fig. 9 TEM images and particle size distribution of fresh and used catalysts: (a) fresh Pd/Ts-1; (b) used Pd/Ts-1; (c) fresh Pd/Al<sub>2</sub>O<sub>3</sub> and (d) used Pd/Al<sub>2</sub>O<sub>3</sub>.

are provided in Table 3. Prior to analysis, the fresh sample was calcined in air at 500 °C for 2 h, while the used sample was from

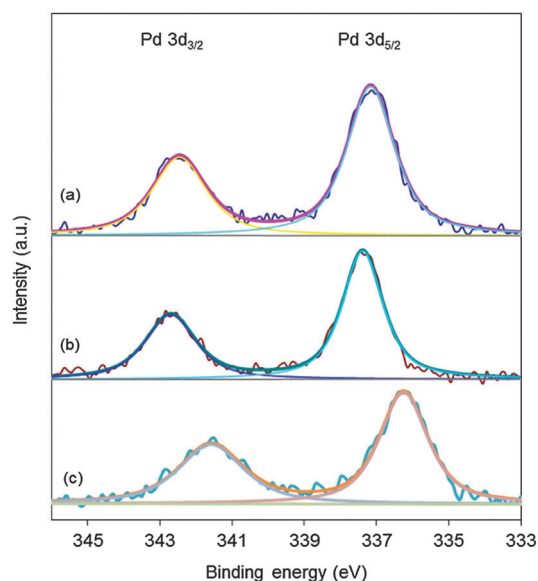


Fig. 10 XPS spectra of Pd 3d core level of (a) fresh Pd/Ts-1, (b) used Pd/Ts-1 and (c) used Pd/Al<sub>2</sub>O<sub>3</sub> catalysts.

the long term (1900 h) stability tests as plotted in Fig. 3. The spectra of the fresh catalyst sample (Fig. 10a) reveals a single distinct peak representing the Pd 3d<sub>5/2</sub> core level transitions, similar to what can be observed from the used sample (Fig. 10b). No metallic Pd was detected from the surface of the used sample. The presence of PdO<sub>2</sub> at binding energies of 337.2–337.4 eV has been assigned by comparing with shifts reported in the literature<sup>40–42</sup> with the oxide most likely formed during calcination of Pd/Ts-1 catalyst. The unique formation of Pd<sup>4+</sup> on zeolite supported Pd catalyst has been confirmed by Bi and Lu who studied Pd/NaZSM-5 calcined at 600 °C where a binding energy was observed at 337.7 eV.<sup>43</sup> On the other hand, they also observed that upon calcination of Pd/Al<sub>2</sub>O<sub>3</sub>, the binding energy of Pd 3d<sub>5/2</sub> was 336.6 eV (which can be identified as Pd<sup>2+</sup>), relatively similar to what was found from our Pd/Al<sub>2</sub>O<sub>3</sub> catalysts (Fig. 10c). XAS investigations are currently underway to unequivocally identify the state of the Pd functionality. This suggests the formation of Pd<sup>4+</sup> on Pd/Al<sub>2</sub>O<sub>3</sub> catalysts is unlikely. Meanwhile, palladium supported on zeolite can stabilize the presence of PdO<sub>2</sub> through the special space structure of the zeotype.<sup>43</sup>

The binding energy of a peak at Pd 3d<sub>5/2</sub> core level of the time-on-stream used catalyst (Fig. 10b) is shifted 0.2 eV towards a higher BE compared to the fresh catalyst. However, the shape of deconvoluted peak at Pd 3d<sub>5/2</sub> core level of the used catalyst

Table 3 Surface composition and binding energies at Pd 3d core level

Sample	Pd 3d <sub>5/2</sub> peak position (eV)	Surface composition (%)					
		Pd	O	Ti	Si	Al	C
(a) Pd/TS-1, fresh	337.2	0.5	64.1	0.3	33.1	—	2.12
(b) Pd/TS-1, used	337.4	0.3	63.6	0.2	32.7	—	3.12
(c) Pd/Al <sub>2</sub> O <sub>3</sub> , used	336.3	0.2	59.2	—	—	—	37.1

is virtually identical to the fresh catalyst peak pattern. As shown in Table 3, the ratios of Pd to Ti or Pd to Si are similar for used and fresh catalyst. In addition, comparison of a plot of Ti 2p core-level of fresh and used Pd/TS-1 spectra (see Fig. S6 and Table S1 of ESI<sup>†</sup>) indicates no shift in binding energy. These suggest no significant changes in chemical/oxidation state of Pd/TS-1 catalyst following the long term operation under surrogate VAM gas, and that the Pd phase in Pd/TS-1 catalyst is stable and less sensitive to water poisoning as no other species was able to be detected from this spectra. In contrast, Pd on alumina shows significant variation of the Pd signature<sup>2</sup> which can be attributed to the formation of palladium hydroxide. The argument is inline with TPD plots (Fig. 6 and 7) as well as the comparison bed furnace temperatures plotted in Fig. 3.

## 4. Conclusion

The catalytic activity and stability of palladium supported on TS-1 catalyst was investigated in catalytic combustion of a lean methane/air mixture and compared with Pd/Al<sub>2</sub>O<sub>3</sub> catalyst. A notable increase in hydrothermal stability was observed over 1900 h time-on-stream experiments, where a constant steady state activity to obtain 90% conversion was achieved below 500 °C. The Arrhenius plot of Pd-TS-1 catalyst obtained after long-term stability test indicates two linear regions with different apparent activation energies and consequently a change in the oxygen surface coverage dependent on the reaction temperature is proposed. Catalyst characterization suggests that water adsorption and in turn the hydrophobicity of the catalyst support plays important role in enhancing the stability of the catalyst. The data obtained disclose that the activity of Pd/TS-1 catalyst was hindered at lower temperature by water present in the feed, however at temperatures higher than 350 °C water is not present on the surface resulting in a lower activation energy compared to Pd/Al<sub>2</sub>O<sub>3</sub>. The hydrophobic properties of titanium silicalite support helps in preventing the accumulation of hydroxyl on the support and also increase the amount of available oxygen.

## Acknowledgements

We duly acknowledge the financial support from ACARP. A. S. thanks the Aceh Province Government, Indonesia for their sponsorship. We thank Jane Hamson for assistance with ICP analysis and Gizelle Sanchez Combata for her help in TPD calibration. We are grateful to University of Newcastle for XRD, SEM and TEM analyses at EM/X-ray unit, and the Australian Synchrotron for the use of their facilities.

## References

- 1 P. Gelin and M. Primet, *Appl. Catal., B*, 2002, **39**, 1–37.
- 2 A. Setiawan, J. Friggieri, E. M. Kennedy, B. Z. Dlugogorski and M. Stockenhuber, *Catal. Sci. Technol.*, 2014, **4**, 1793–1802.
- 3 R. Burch, F. J. Urbano and P. K. Loader, *Appl. Catal., A*, 1995, **123**, 173–184.
- 4 Y. Liu, S. Wang, T. Sun, D. Gao, C. Zhang and S. Wang, *Appl. Catal., B*, 2012, **119–120**, 321–328.
- 5 D. Gao, S. Wang, C. Zhang, Z. Yuan and S. Wang, *Chin. J. Catal.*, 2008, **29**, 1221–1225.
- 6 C. Shi, L. Yang and J. Cai, *Fuel*, 2007, **86**, 106–112.
- 7 F. H. Ribeiro, M. Chow and R. A. Dallabetta, *J. Catal.*, 1994, **146**, 537–544.
- 8 D. Ciuparu, N. Katsikis and L. Pfefferle, *Appl. Catal., A*, 2001, **216**, 209–215.
- 9 W. R. Schwartz, D. Ciuparu and L. D. Pfefferle, *J. Phys. Chem. C*, 2012, **116**, 8587–8593.
- 10 D. P. Serrano, G. Calleja, J. A. Botas and F. J. Gutierrez, *Sep. Purif. Technol.*, 2007, **54**, 1–9.
- 11 M. Taramasso, G. Perego and B. Notari, *US Pat.*, US 4410501, United States, 1983.
- 12 F. Qiu, X. Wang, X. Zhang, H. Liu, S. Liu and K. L. Yeung, *Chem. Eng. J.*, 2009, **147**, 316–322.
- 13 B. Notari, *Catal. Today*, 1993, **18**, 163–172.
- 14 K. Mori, Y. Miura, S. Shironita and H. Yamashita, *Langmuir*, 2009, **25**, 11180–11187.
- 15 I. Moreno, N. F. Dummer, J. K. Edwards, M. Alhumaimess, M. Sankar, R. Sanz, P. Pizarro, D. P. Serrano and G. J. Hutchings, *Catal. Sci. Technol.*, 2013, **3**, 2425–2434.
- 16 S. Specchia, P. Palmisano, E. Finocchio, M. A. L. Vargas and G. Busca, *Appl. Catal., B*, 2009, **92**, 285–293.
- 17 G. D. Carlo, G. Melae, N. Kruse and L. F. Liotta, *Chem. Commun.*, 2010, **46**, 6317–6319.
- 18 P. Castellazzi, G. Groppi and P. Forzatti, *Appl. Catal., B*, 2010, **95**, 303–311.
- 19 J. R. Anderson and K. C. Pratt, *Introduction to characterization and testing of catalysts*, Academic Press, Sydney, Orlando, 1985.
- 20 S. Su, H. Chen, P. Teakle and S. Xue, *J. Environ. Manage.*, 2008, **86**, 44–62.
- 21 J. C. van Giezen, F. R. van den Berg, J. L. Kleinen, A. J. van Dillen and J. W. Geus, *Catal. Today*, 1999, **47**, 287–293.
- 22 K.-I. Fujimoto, F. H. Ribeiro, M. Avalos-Borja and E. Iglesia, *J. Catal.*, 1998, **179**, 431–442.
- 23 D. Ciuparu and L. Pfefferle, *Appl. Catal., A*, 2001, **209**, 415–428.
- 24 D. L. Trimm and C.-W. Lam, *Chem. Eng. Sci.*, 1980, **35**, 1405–1413.
- 25 G. Li, P. Xiao and P. Webley, *Langmuir*, 2009, **25**, 10666–10675.
- 26 G. D. Zakumbaeva and S. V. Artamonov, *React. Kinet. Catal. Lett.*, 1979, **10**, 183–186.
- 27 H. Lynggaard, A. Andreasen, C. Stegelmann and P. Stoltze, *Prog. Surf. Sci.*, 2004, **77**, 71–137.
- 28 C. F. Cullis and B. M. Willatt, *J. Catal.*, 1983, **83**, 267–285.
- 29 T. R. Baldwin and R. Burch, *Appl. Catal.*, 1990, **66**, 359–381.

- 30 B. Stasinska, A. Machocki, K. Antoniak, M. Rotko, J. L. Figueiredo and F. Goncalves, *Catal. Today*, 2008, **137**, 329–334.
- 31 D. V. Ivanov, L. G. Pinaeva, L. A. Isupova, E. M. Sadovskaya, I. P. Prosvirin, E. Y. Gerasimov and I. S. Yakovleva, *Appl. Catal., A*, 2013, **457**, 42–51.
- 32 J. B. Peri, *J. Phys. Chem.*, 1966, **69**, 220–230.
- 33 M. Zamora and A. Cordoba, *J. Phys. Chem.*, 1978, **82**, 584–588.
- 34 M. Egashira, M. Nakashima, S. Kawasumi and T. Seiyama, *J. Phys. Chem.*, 1981, **85**, 4125–4130.
- 35 R. S. Drago, S. C. Dias, J. M. McGilvray and A. L. M. L. Mateus, *J. Phys. Chem. B*, 1998, **102**, 1508–1514.
- 36 K. S. W. Sing, *Pure Appl. Chem.*, 1982, **54**, 2201–2218.
- 37 D. P. Serrano, R. Sanz, P. Pizarro, I. Moreno and S. Medina, *Appl. Catal., B*, 2014, **146**, 35–42.
- 38 D. L. Trimm, in *Studies in Surface Science and Catalysis*, ed. H. B. Calvin and B. B. John, Elsevier, 1991, pp. 29–51.
- 39 J. H. Lee and D. L. Trimm, *Fuel Process. Technol.*, 1995, **42**, 339–359.
- 40 D. Gao, C. Zhang, S. Wang, Z. Yuan and S. Wang, *Catal. Commun.*, 2008, **9**, 2583–2587.
- 41 A. M. Venezia, G. Di Carlo, G. Pantaleo, L. F. Liotta, G. Melaet and N. Kruse, *Appl. Catal., B*, 2009, **88**, 430–437.
- 42 S. P. Chenakin, G. Melaet, R. Szukiewicz and N. Kruse, *J. Catal.*, 2014, **312**, 1–11.
- 43 Y. Bi and G. Lu, *Appl. Catal., B*, 2003, **41**, 279–286.